



**HAL**  
open science

## Quantitative mapping of high modulus materials at the nanoscale: comparative study between atomic force microscopy and nanoindentation

Rosine Coq Germanicus, D. Mercier, F. Agrebi, M. Fèbvre, D. Mariolle, Ph. Descamps, Ph. Leclère

### ► To cite this version:

Rosine Coq Germanicus, D. Mercier, F. Agrebi, M. Fèbvre, D. Mariolle, et al.. Quantitative mapping of high modulus materials at the nanoscale: comparative study between atomic force microscopy and nanoindentation. *Journal of Microscopy*, 2020, 280 (1), pp.51-62. 10.1111/jmi.12935 . hal-03343212

**HAL Id: hal-03343212**


**<https://hal.science/hal-03343212>**

Submitted on 10 Jun 2023

**HAL** is a multi-disciplinary open access archive for the deposit and dissemination of scientific research documents, whether they are published or not. The documents may come from teaching and research institutions in France or abroad, or from public or private research centers.

L'archive ouverte pluridisciplinaire **HAL**, est destinée au dépôt et à la diffusion de documents scientifiques de niveau recherche, publiés ou non, émanant des établissements d'enseignement et de recherche français ou étrangers, des laboratoires publics ou privés.

# Quantitative mapping of high modulus materials at the nanoscale: comparative study between atomic force microscopy and nanoindentation

R. COQ GERMANICUS\* , D. MERCIER†, F. AGREBI\*, M. FÈBVRE‡, D. MARIOLLE§, Ph. DESCAMPS|| & Ph. LECLÈRE#

\*Normandie Univ, UNICAEN, ENSICAEN, IUT, CNRS, CRISMAT, Caen 14000, France

†CRM Group, Liège, Belgium

‡Bruker, Nano Surfaces, Palaiseau, France

§CEA, LETI, UNIV, Grenoble Alpes, Grenoble, France

||UNIROUEN, ESIGELEC, IRSEEM, Normandie UNIV, Rouen, France

#CIRMAP, Service de Chimie des Matériaux Nouveaux, Université de Mons (UMONS), Mons, Belgium

**Key words.** Atomic Force Microscopy (AFM), hardness, nanoindentation, peak force quantitative nanomechanical mapping (PF-QNM), silica beads, Young's modulus.

## Summary

Local mechanical properties of submicron features are of particular interest due to their influence on macroscopic material performance and behaviour. This study is focused on local nanomechanical measurements, based on the latest Atomic Force Microscopy (AFM) mode, where the peak force set point is finely controlled at each pixel. After probe calibration, we evaluate the impact of spring constant of two AFM hand-crafted natural full diamond tips with steel cantilevers, used for mapping. Based on the fast capture of the cantilever deflection at each pixel and real time force curve analysis in the elastic region, AFM local measured contact moduli mappings of the silica beads (> 50 GPa) incorporated in an epoxy resin matrix, are compared with those determined using classical instrumented nanoindentation tests. Our analyses show that with the two AFM probes, without local residual deformation, the high moduli of the silica beads measured with this advanced AFM mode are within the standard deviation of the values determined by classical nanoindentation.

## Introduction

For several decades, Atomic Force Microscopy (AFM) technique proves their powerful and unique ability of providing 3D mappings of various material properties. Based on the

AFM tip-sample interaction, the surface topography is characterised with a high sensitivity typically better than 0.05 nm in the  $z$ -direction with a nanometric spatial resolution (in  $x$ - and  $y$ -directions). In addition, different techniques were deployed to access chemical (Balnois *et al.*, 2007; Huang *et al.*, 2016), electrical (Coq Germanicus *et al.*, 2007; Eyben *et al.*, 2007; Murray *et al.*, 2007; Coq Germanicus *et al.*, 2015; Vandervorst *et al.*, 2017; Germanicus *et al.*, 2020) and also local mechanical properties (Heuberger *et al.*, 1995; Pittenger *et al.*, 2014) with the same spatial resolution. For the local mechanical properties, the classical force volume AFM mode allows to collect, at each pixel, the force–separation curves to deduce the elastic properties, namely the stiffness and the adhesion. Nevertheless, the acquisition process of data in this mode drastically limits the measurements with very low imaging speeds and resolution (Smolyakov *et al.*, 2016).

Based on faster captures and real time force curve analysis, advanced nanomechanical nonresonance intermittent contact modes are developed on AFM. In this AFM mode, an oscillation at several kilohertz, well below its resonance frequency is applied on the cantilever, at which the classical tapping topography mode usually operates. The probe is brought intermittently into contact with the sample surface in the normal direction during a short period (<100  $\mu$ s) to minimise lateral forces. The main strength of the Peak Force Quantitative Nanomechanical Mapping (PF-QNM) (Fischer *et al.*, 2013) is that the maximum applied force, also called the peak force setpoint, is precisely controlled over the instantaneous interaction and is maintained constant in the feedback loop for each pixel of the mapping. This control limits the sample deformation to few nanometres and allows the

Correspondence to: R. Coq Germanicus, Normandie Univ, UNICAEN, ENSICAEN, IUT, CNRS, CRISMAT, Caen F-14000, France. Tel: +33 2 31 56 71 41; e-mail: rosine.germanicus@unicaen.fr

fine control of tip-sample interaction. Then at each pixel of the scanned area, the force–distance curve is then recorded. Therefore, PF-QNM which is a higher speed mode improves the scan rate (less than 1 line  $s^{-1}$ ), force resolution (about  $10^{-10}$  N) and reduces the noise signal. From the recorded PF-QNM force curves, simultaneously to the topography, quantitative nanomechanical properties such as the deformation, indentation, dissipation, adhesion and contact modulus are quantified and then mapped. All mechanical properties are deduced from the deflection of the cantilever when the AFM probe is in interaction with the sample surface. PF-QNM results for materials such as polyurethane and poly(styrene) samples (Dokukin & Sokolov, 2012), different polymers with a range of Young's moduli from low-density poly(ethylene) (0.2 GPa) to poly(methyl methacrylate) (3 GPa) (Young *et al.*, 2011), flax fibre cell walls (Arnould *et al.*, 2017), poly (L-Lactic Acid) nanofibres (Cuong *et al.*, 2020), bitumen (Fischer *et al.*, 2013), organic matter of Bakken Shale (Li *et al.*, 2018), nanobubbles (Walczyk *et al.*, 2013) and also living bacteria (Smolyakov *et al.*, 2016) with elastic modulus (from several MPa to 10 GPa) relatively low, have been reported. For relatively high Young's modulus ( $> 50$  GPa), first results are published in 2014 on polished glass surfaces (Hopf & Pierce, 2014).

Moreover, some publications showed that PF-QNM revealed to be a powerful tool to characterise the mechanical properties of composite materials with biopolymer in particular to characterise cellulose nanowhiskers (Khelifa *et al.*, 2013), chitin nanorods (Smolyakov *et al.*, 2016) and polymer bends (Bahrami *et al.*, 2019). More recently, a report (Qi *et al.*, 2019) analysed the interphase properties in carbon fibre reinforced epoxy matrix. They evaluate the effective thickness of the interface using a silicon cantilever with spring constant of  $40 \text{ N m}^{-1}$ .

For higher values of local elastic modulus ( $> 10$  GPa), only few studies address the capability of PF-QNM measurements. In (Trtik *et al.*, 2012), cement pastes are analysed, the authors showed that PF-QNM can be determined the Young's modulus only by using a diamond probe mounted on a cantilever with a spring constant of  $212 \text{ N m}^{-1}$ . Young's modulus of nanostructured bainitic steel (Morales-Rivas *et al.*, 2015) were analysed by PF-QNM. Finally, based on the underexplored research on AFM mechanical mappings for rigid material, Zeng *et al.* (2018) present experimental results obtained for bulk material: fused silica, highly oriented pyrolytic graphite (HOPG), silicon and gold. They studied the noise level of the PF-QNM, the evolution of the applied force and the impact of the tip radius. They show the low noise level of the PF-QNM and the need to apply enough force to obtain sufficient large contact area while remaining in the elastic range, to reach a certain measurement accuracy. Local mechanical properties of submicron features are of particular interest due to their influence on macroscopic material properties and behaviour (Dittanet & Pearson, 2012).

Encapsulation of epoxy matrix also called Epoxy Moulding Compound (EMC) is widely used as plastic packages for automotive, aerospace coatings and integrated microelectronic devices (Rector *et al.*, 2000; Liu *et al.*, 2004). In fact, plastic packaging ensures electrical insulation and protects the electronic devices from external environment (Kim *et al.*, 2010; Wong *et al.*, 2016). With EMC encapsulation material, the integrated semiconductor chips are physically protected from temperature, moisture, stress and chemical attacks. During the packaging process, EMC's are thermally cured above or around the microelectronic devices. Then for this thermosetting polymer, in addition to the composition of the polymer matrix, a good combination of chemical, thermal, electrical and mechanical properties (Liu *et al.*, 2004; Tsai *et al.*, 2006) must be optimised to reach the maximum of packaging target properties. Two main aspects must be considered: the specific properties of the material (Bae *et al.*, 2004; Zhang & Wong, 2004) but also the reliability of the package (Lu *et al.*, 2009; Noijen *et al.*, 2009; Tachapitunsuk *et al.*, 2017; Oh *et al.*, 2019) in contact with the semiconductor chip (Gan *et al.*, 2014). Usually, the epoxy material is used for its good fluidity (Linec & Mušič, 2019), curing property and the capability to design integrated 3D shapes. To improve mechanical properties (Wang *et al.*, 2002; Sriwithoon *et al.*, 2017), electrical properties (Bell *et al.*, 2017; Chandra *et al.*, 2019) and control thermal dissipation, the epoxy resin is filled by silicon dioxide beads, also called nanosilica particles (Preghenella *et al.*, 2005; Liang & Pearson, 2009; Dittanet & Pearson, 2012). For microelectronic applications silica beads added in the EMC material represent an ingredient with a proportion more than 50 Vol %. Therefore, a control of the beads distribution and local properties allows to optimise the encapsulation processing.

In this paper, local mechanical properties at the nanoscale of EMC material used for microelectronic package is studied by PeakForce QNM. Silica beads incorporated in epoxy matrix represents an interesting material to evaluate the capability and analyse results of PF-QNM mode. We focus on the deployed method to discriminate the high modulus values of silica beads. For that, two dedicated specific and AFM hand-crafted natural diamond tips with steel cantilevers are considered. After the calibration of the diamond triangular pyramid probes, the impact of cantilever spring constant on the all PF-QNM AFM signals is analysed and discussed. Furthermore, the modulus values obtained from PF-QNM were compared with classical depth-sensing instrumented nanoindentation mapping tests.

## Materials description and experimental methods

### *Epoxy moulding compound*

During the encapsulation process, semiconductor circuits are placed in the cavity of a moulding machine. The thermosetting polymer Epoxy Moulding Compound is injected into pellet

form into the mould cavity containing the semiconductor chip (Han & Wang, 1997; Zhang & Wong, 2004). The moulding process is performed at an elevated pressure and elevated temperature around 170°C. After this packaging step, the EMCs with the semiconductor's dies are thermally cured to obtain the device packaged.

The studied matrix is an epoxy o-cresol novolac resins (10 % of the weight), which contains 8 % of phenol novolac group (hardener and curing agents) filled with 80 % of silica beads. Inorganic fillers, glass fibres, pigments compose also the EMC material. Then the encapsulation material consists to a mixture of an epoxy resin, curing agents, silica filler, hardener, pigments like carbon black and other additives. For our analysis, specimens were hand-polished with lapping films of decreasing granularity to access and analyse the surface of the cross section of the EMC packaging.

#### Nanoindentation tests

Classical depth-sensing instrumented nanoindentations tests (Doerner & Nix, 1986; Pharr & Oliver, 1992; Baker, 2001) are currently deployed to determine local mechanical properties as a function of the depth penetration in material at a micrometric scale. This technique is based on the measurement of the vertical applied load on a hard indenter which penetrates perpendicularly the surface of the sample. From the vertical indenter displacement (also called penetration depth), the curve force–displacement is generated, with a displacement sensitivity about 1 nm and a load sensitivity better than 10 nN (Cohen & Kalfon-Cohen, 2013). From experimental data, models allow to determine the mechanical properties of the studied material such as the hardness and the Young's modulus. For stiff materials, the widely used method is the Oliver and Pharr model (Oliver & Pharr, 1992). Several publications prove the capability and sensitivity of the instrumented nanoindentation tests for the determination of the intrinsic mechanical parameters for single materials (Lin *et al.*, 2009), thin films deposited on substrate (Li & Vlassak, 2009) (Bae *et al.*, 2004) (Liu *et al.*, 2015) and composite materials (Ho & Marcolongo, 2005; Ureña *et al.*, 2005; Kossman *et al.*, 2019; Mercier *et al.*, 2019).

Nanoindentation measurements were made using an Agilent Nano Indenter G200–XP head at room temperature at an acquisition frequency of 10 Hz. The continuous stiffness measurement (CSM) mode is used (Li & Bhushan, 2002). In this dynamic CSM mode, an oscillation, of 0.5 nm at a frequency of 75 Hz, is superimposed on the load signal, allowing for a continuous monitoring of the surface stiffness. Therefore, load ( $L$ ), displacement ( $h$ ) and elastic contact stiffness ( $S$ ) were continuously recorded during indentation. Mechanical properties are determined from the unloading force–displacement curve. The area function ( $A_c$ ) of the contact depth was carefully calibrated based on nanoindentation tests on bulk fused silica and obtained using the contact depth equation from Oliver and

Pharr (Oliver & Pharr, 1992). Nanoindentation experiments were load-controlled with a maximal force set at 4 mN. Elastic modulus was estimated using the well-known modified Sneddon's relationship given by Eqs. (1) and (2), with a geometrical correction factor ( $\beta$ ) equal to 1.034, and the hardness ( $H$ ) was obtained using Eq. (3).

$$E_r = \frac{S}{2\beta} \sqrt{\frac{\pi}{A_c}}. \quad (1)$$

The sample Young's modulus ( $E_s$ ), is related to the reduced Young's modulus ( $E_r$ ), given by

$$E_s = (1 - \nu_s^2) \left[ \frac{1}{E_r} - \frac{(1 - \nu_{Tip}^2)}{E_{Tip}} \right]^{-1}, \quad (2)$$

where  $\nu_s$  and  $\nu_{Tip}$  are the Poisson's ratios of the sample and the tip respectively. For silica,  $\nu_s$  is fixed at 0.17. Since the tip is made in diamond (very high elastic modulus about 1 TPa and low [0.07] Poisson's ratio), the term for the indenter in (2) can be neglected.

$$H = \frac{L}{A_c}. \quad (3)$$

To evaluate variability, targeted nanoindentation tests are carried out on silica beads.

#### AFM and PeakForce QNM analysis

PeakForce Tapping mode with quantitative nanomechanical analysis were performed using a Dimension Icon instrument from Bruker, driven by a Nanoscope V. For the mechanical PF-QNM mode, we selected two hand-crafted natural diamond AFM probes where the apex is the corner of a cube so that three right angle planes. They can therefore be compared to cubic indenters. These two ultrahigh strength triangular pyramid tips are fabricated by accurate grinding of a solid diamond. The steel material used for cantilevers presents two very high spring constants. Chosen for its the material stability and mechanical resistance, these tips are designed for nanomechanical measurement. Calibrations and parameters of the used probes are determined and given in the next part.

For all measurements, the cantilever oscillates with a resonant frequency of 1.9 kHz, under ambient conditions at room temperature. The line scan rate was equal to 0.50 Hz, all maps (topography and mechanical properties) are obtained in roughly 17 min.

In addition, topographic image in Tapping mode, a monolithic silicon tip (NCH,  $k = 40 \text{ N m}^{-1}$  and  $f_0 = 320 \text{ kHz}$ ) with a smaller radius of 10 nm is used. The resonance frequency is 320 kHz. The image scan rate was 1 Hz and the image resolution was  $512 \times 512$  pixels. This AFM Tapping mode tip is used to quantify the surface roughness and to image residual plastic imprints after nanoindentation tests.

**Table 1.** Properties of the used tips and parameters for PF-QNM.

Tip reference	DNISP	DNISP-HS
Geometry $L, W, e$ ( $\mu\text{m}$ )	350, 100, 13	350, 100, 13
Probe material	Full diamond	Full diamond
Effective probe radius (nm)	57	62
Cantilever material	Stainless steel	Stainless steel
Deflection sensitivity ( $\text{nm V}^{-1}$ )	$81.8 \pm 0.3$	$70.5 \pm 1.9$
Spring constant ( $\text{N m}^{-1}$ )	292	393
Peak force ( $\mu\text{N}$ )	0.7	1

## Results and discussion

### Calibration

Nowadays for obtaining higher sensitivity of mechanical properties in micro-nanoscale with excellent local characterisations, two techniques based on probe (or tip)–sample interactions were used: instrumented nanoindentation and mechanical measurements on AFM (Cohen & Kalfon-Cohen, 2013). Difference between the two probe techniques arise from tip size, reliable characterisation of force, dynamic range, force application mechanism depth penetration range and displacement sensitivity (Cohen & Kalfon-Cohen, 2013).

Nanoindentation tests were carried out with a sharp pyramid-shaped Berkovich diamond indenter tip. The tip radius of the three-sided pyramid (face angle of  $65.3^\circ$ ) Berkovich tip is 20 nm.

To obtain mechanical properties from PF-QNM force curve, the tip must be able to induce sample deformation while reducing its own deformation. The probe mounted on the cantilever must be harder than the analysed materials. Then, high spring constant of the cantilever is necessary to access to the relative high value of the elastic modulus. Therefore, the Young's modulus of the probe and cantilever spring constant of the used tip are two critical parameters for PF-QNM. We used two cube-corner hand-crafted natural diamond AFM probes: DNISP (probe 1) and DNISP-HS (probe 2). These two tips, with a height of  $50 \mu\text{m}$ , are selected for their high Young's moduli  $> 50 \text{ GPa}$ . The geometries (length, width and thickness) of these steel cantilevers are indicated Table 1. For quantitative measurements, in order to estimate the force applied by the AFM probe, we must determine the deflection sensitivity and the spring constant of the cantilever. The deflection sensitivity quantifies the response of the AFM photodetectors when the cantilever deflects. For this, we measured the cantilever sensitivity from the slope of the force curve when the tip interacts with the surface of a sapphire sample. Results are done in Table 1, in addition for comparison we have added the values obtained for a silicon tip coated with aluminum. The spring constants are determined by the accurate Laser Doppler Vibrometry (LDV) method. With this method, the associated uncertainty in the calibrated spring constants is about 5%. This

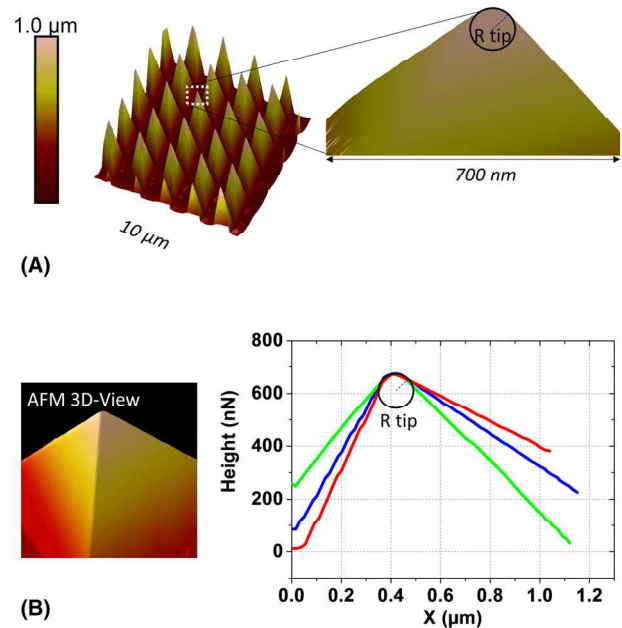


**Fig. 1.** Determination of the AFM tip radius for the hand-crafted natural diamond probe (A) AFM topography of the calibration grating TGT1, (B) 3D-AFM view of the apex and profiles on the top of the image of the AFM Berkovich tip.

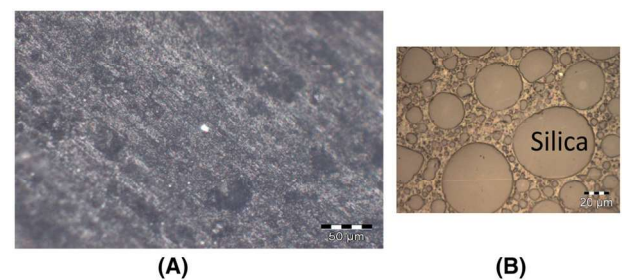


**Fig. 2.** Surface of the studied sample, (A) before and (B) after hand-polishing.

calibration is obtained by multiplying the deflection of the cantilever by the cantilever spring constant, a calibration step of the deflection sensitivity is necessary. In addition, it's essential to know the tip radius of the used probes to determine the effective Young's modulus. For that, a calibration procedure is achieved in three steps: two absolute procedures and a relative procedure with reference samples of known modulus is also performed to increase the accuracy.

In a first step, the deflection sensitivity of probes was determined with ramp force curves taken on a sapphire. Second, the real tip shapes and radius are determined with the calibration grating TGT1 from NT-MDT sample (Xu *et al.*, 2018). This calibration sample consists a 3D-array of cone-shaped silicon spikes with curvature radius less than 10 nm. From a topography scan of the 3D-array, effective tip radius is

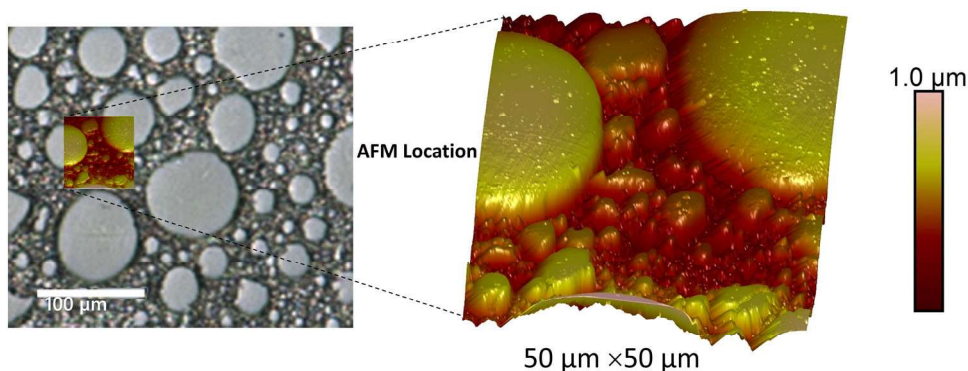


Fig. 3. Top-view optical microscopy image and surface topology of the EMC obtained by AFM in tapping mode.

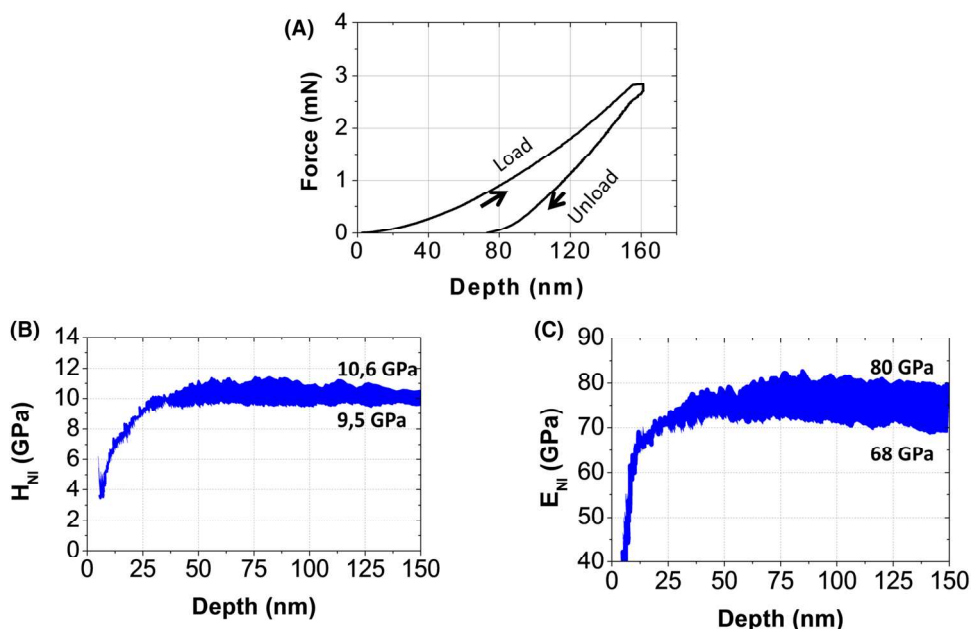


Fig. 4. Results of classical nanoindentation (A) typical load–displacement curve, (B) hardness ( $H_{NI}$ ) and (C) elastic modulus ( $E_{NI}$ ) determined in locations of the silica beads as a function of the depth penetration. The range of  $E_{NI}$  and  $H_{NI}$  values for silica from the nanoindentation matrix are represented.

obtained from the inverse image technique (Xu *et al.*, 2018). In fact, by scanning the grid, the tip is imaged as the sample features are sharper as those of the probe used. Results for the DNISP tip are shown in Figure 1, for a scan size of  $10\ \mu\text{m} \times 10\ \mu\text{m}$  with  $512 \times 512$  pixels. The topography of the 3D-array conical structure shows a grid of regular triangular pyramid shapes attesting that the AFM acquisition corresponds to the real shape of the three face of the corner cube diamond probe. We can see in Figure a zoomed view ( $700\ \text{nm} \times 700\ \text{nm}$ ), showing that the tip apex is a quasi-spherical shape. The real tip radius determined at 57 nm and 62 nm for probe 1 and probe 2 respectively were similar. These relatively high values for AFM tip radius are necessary to ensure a large and stable

contact between the tip and the sample and to provide elasticity properties (Zeng *et al.*, 2018).

Finally, to adjust the experimental settings of the PF-QNM mode, for each probe, two reference samples with known Young's modulus: Al (80 GPa) and Si (165 GPa) are considered. The applied peak force and the feedback signal for each probe were then fixed. Table 1 indicates the main properties of the two used probes and their PF-QNM parameters. Since the spring constants of the two tips are different, a higher force must be applied for the probe 2 (DNISP-HS) with the higher spring constant to achieve the same deformation. Indeed, in this study, we fixed the indentation to try to have the same value of  $A_c$  (see Eq. (1))

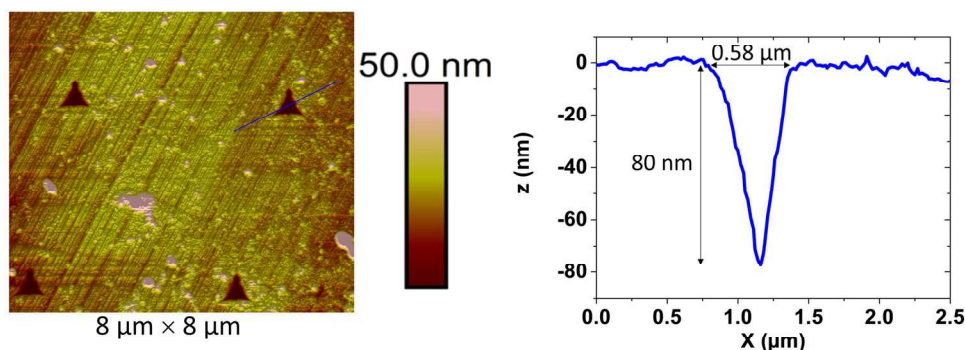


Fig. 5. AFM topography of residual indents after classical instrumented nanoindentation tests with a maximum penetration depth of 200 nm. The AFM scan size is  $8 \times 8 \mu\text{m}^2$ , the cross sectional profile indicates the residual width and depth of the indent.

### Surface characterisation

For an accurate characterisation, a very smooth surface of EMC is necessary. As presented before, the EMC are prepared with hand-polishing. Optical microscopy images of the sample before and after preparation are done in Figure 2. After hand-polishing, we can easily distinguish the micro-sized filler in the polymer: silica beads incorporated in the epoxy matrix.

The AFM topography of the EMC is represented in Figure 3, for a scan size of  $50 \times 50 \mu\text{m}^2$ . We can observe that the filler consists on a multimodal silica beads distribution (diameters from a few micrometres to  $90 \mu\text{m}$ ), assuring a high filler loading. The large beads are separated by smaller ones incorporated in the epoxy matrix. Therefore, the spherical shape of the beads is highlighted; this shape increases the EMC viscosity during the moulding step. The multimodal size distribution of the silica beads in the matrix has a significant effect on thermal properties, fracture toughness and global Young's modulus of the material (Dittanet & Pearson, 2013). The AFM topography shows that fused silica dusts strengthen the epoxy matrix. Due to the intrinsic resistances to abrasion of the silica beads, silica dusts and epoxy matrix of the EMC, a topography is induced by the polishing step, the 3D view is represented in Figure 3. However, locally in the surface of the silica beads, the average roughness  $R_a$  of 15 nm and the root mean squared (RMS) roughness  $R_q$  of 18 nm are obtained. Compared to the tip apex, these results are quite suitable for considering a constant sample tip contact when the probe indents the silica beads surface.

### Mechanical properties: classical nanoindentation and PF-QNM

Classical instrumented nanoindentation tests were performed. Figure 4 presents a typical load–displacement curve obtained, with CSM mode. The curve shows an elastic plastic deformation. The mechanical parameters, ( $E_{NI}$ ) and ( $H_{NI}$ ) of the silica beads are plotted as a function of the depth penetration (Figs. 4B and C) for a maximum depth penetration of 150 nm. At smaller penetration depths ( $<30 \text{ nm}$ ), the sharp

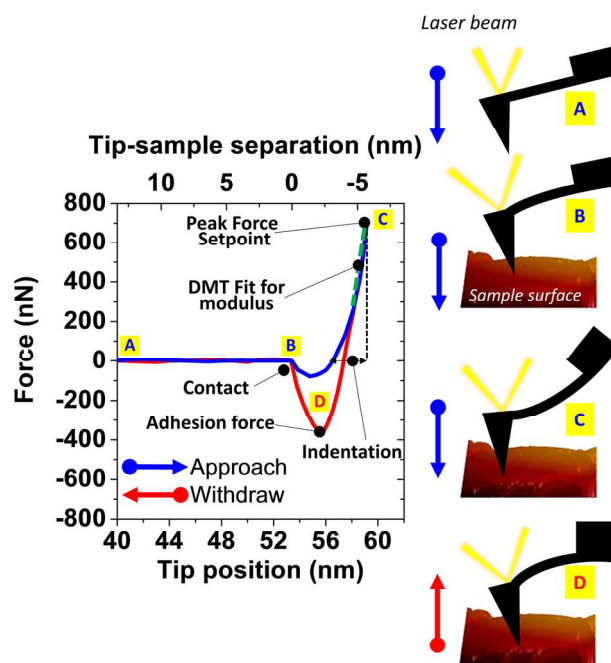


Fig. 6. Schematic of cantilever position during the PF-QNM stage and force–tip position (or sample separation) curve acquired on a silica bead obtained with tip 1.

increase of mechanical properties is attributed to surface or skin effects. Around 100 nm, the curves present a plateau where the hardness and elastic modulus reach mean values of about 10 and 74 GPa, respectively. These values are in agreement with the results reported for silica bulk in the literature (Granta, 2019). The variation of the measured Young's modulus values can be explained by the size distribution of elastic beads and the elastic deformation of the surrounding softer epoxy 2–4.5 GPa (Granta, 2019).

After classical nanoindentation, AFM topographies of a grid of  $2 \times 2$  indents (from the  $16 \times 16$  tests) are performed. The corresponding line scan profiles are represented in Figure 5. The nanoindentation test induced residual indents which are

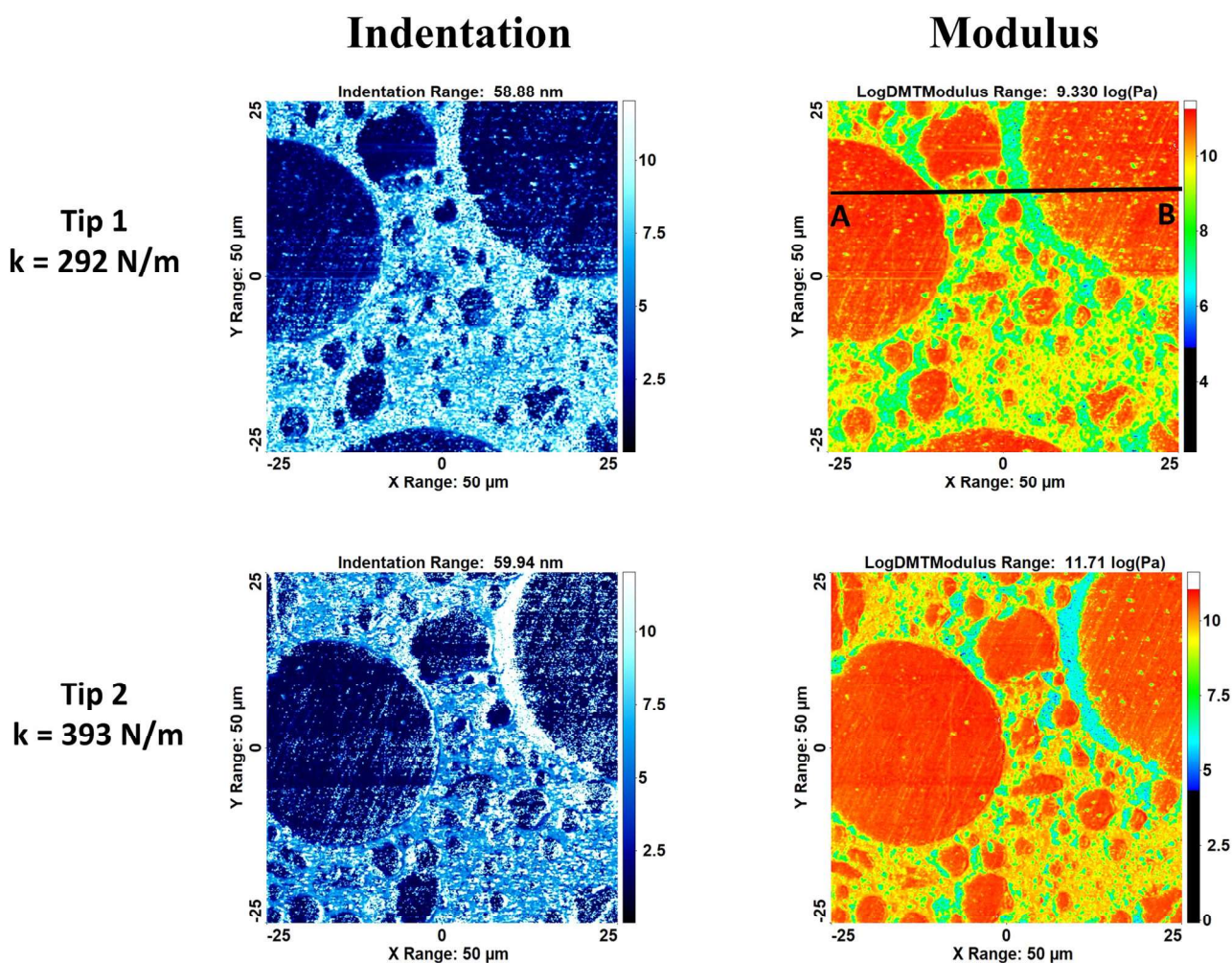


Fig. 7. AFM PF-QNM maps of indentation and DMT modulus obtained with the two hand-crafted natural diamond AFM probes with steel cantilevers. Scan size  $50 \times 50 \mu\text{m}^2$ .

imprinted in the silica beads. Imprints are well-formed with a regular shape in accordance with the Berkovich shape of the nanoindenter. The elastoplastic interaction during the classical nanoindentation is confirmed by the dimension of the residual indent: 80 nm in residual depth (in agreement with load–displacement curve in Figure 4(A) and 0.58  $\mu\text{m}$  in width for a maximum depth penetration of 200 nm during the test.

PeakForce-QNM measurements were used to acquire local mechanical properties of the silica beads, at the same location. AFM tip is intermittently in contact with the surface, in each oscillation cycle a force–displacement curve is recorded. Figure 6 represents a typical force versus probe tip position obtained by acquiring the deflection of the cantilever when the periodically modulated PF-QNM probe interacts with the silica bead. The approach and withdraw stages are indicated in the curve. At the beginning, the diamond probe is located at 50 nm (A) above the silica surface.

Afterwards the cantilever is pulled down towards the surface with the z-piezo to contact the surface of the sample (B). The force increases until the Peak Force Setpoint (700 nN in our experiment) is reached (C). Then, the cantilever starts to withdraw. The applied force decreases, until it reaches a minimum (D), at this point the adhesion signal is determined. During the last step the tip is removed from the surface. A high modulation frequency of 2 kHz (0.5 ms for the force curve) is used.

In our case, as mentioned above, since the depth deformation is lower than the determined real tip radius, the Derjaguin–Muller–Toporov (DMT) stiffness fit model (Derjaguin *et al.*, 1975) is employed to the unloading portion of the curve to calculate the contact modulus at each pixel. This modified Hertzian model considers the adhesive forces between the AFM tip and the sample surface. The DMT fit is applied on the unloading stage of the force–distance curve.



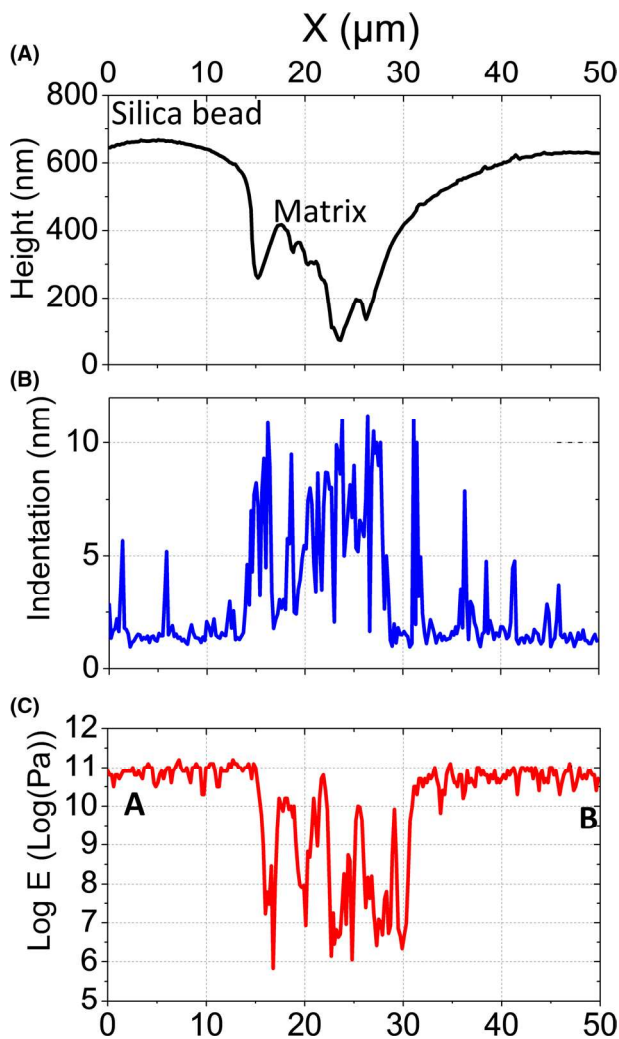


Fig. 8. Profiles along the AB axis, (A) Topography indicates the silica surface, (B) tip Indentation and (C) corresponding Young's modulus drawn for the tip 1.

According to this approach, the Young's modulus of the probed material  $E_r$  is given by

$$E_r = \frac{3}{4} \frac{(F_{tip} - F_{adh})}{\sqrt{Rd^3}}, \quad (4)$$

where  $F_{tip}$  is the force applied on the AFM tip,  $F_{adh}$  is the adhesive force, the two forces are determined from the measured force–distance curve,  $R$  is the AFM tip radius and  $d$  is the sample deformation. The sample Young's modulus ( $E_s$ ) can also be estimated using Eq. (2) and by neglecting tip elastic deformation (because of the high Young's modulus of diamond). Therefore, during the scan, simultaneously to the topography, quantitative mechanical properties are extracted for each pixel, such as adhesion, surface deformation and contact modulus.

Figure 7 presents mappings of the material indentation and contact modulus obtained with PF-QNM analysis with the two

probes at the same location of the sample. We deliberately slightly shifted the scan area for measurements with the second probe to check that we had not damage the surface during the first scan. No surface modification was observed after PF-QNM measurement. Maps of indentation give for each pixel the depth of indentation of the probe into the material. For silica beads, except on the sides, the indentation signal seems to be quite uniform. Then, indentation maps show the stability of the contact during the scan of the silica beads.

Moreover, since the indentation signal is a signature of the hardness of the material, the very low indentation measured on the surface of the silica beads attests the high hardness of the incorporated beads. The modulus maps show the capability of the PF-QNM mode to discriminate and measure relative high modulus with the used probes. Two populations are highlighted, one when the tip is in contact with silica beads and the second one when the pixels fit to the epoxy matrix with fused silica dusts. Profiles along AB axis are presented in Figure 8. The profile of the height allows to localise the silica bead surface, corresponding indentation and modulus signals, respectively. As expected, when the hard PFT-QNM tip is in contact with the matrix, the indentation signal is higher than when the tip is located on the surface of the silica bead surface. We can also note that, by scanning the surface of the silica, the deformation of the cantilever is relatively stable from 1.7 to 2.9 nm.

In order to evaluate the impact of spring constant, histograms of PF-QNM parameters (indentation and Young's moduli signals) corresponding to the whole scanned images are depicted in Figure 9 for the two AFM probes. A low adhesion signal (not show here) on whole the image attested that the surface tested was clean and uncontaminated. For indentation, histograms show a bimodal mode, corresponding to silica and to the epoxy matrix, respectively. The distributions of maximum indentation depth into the material during the elastic PF-QNM measurements show a first narrow peak with a max at 1.2 nm corresponds to the indentation of the diamond probes into the silica materials. Whatever the used probe, the peak is the same, which confirms that the applied forces on the cantilever induce the same elastic deformation in the silica. With this result, we validate the applied calibration steps and experimental settings for each probe. The indentation histograms present also a tail on a broad band. This response is measured for the matrix. Some pixels exhibit very high value of indentation  $>12$  nm. These values correspond to edge of the beads where effective contact area between the tip and the surface is not stable. In Figure 7, the indentation map obtained with the tip 2 shows a crown around the bead where the signal is very high. This crown corresponds to geometric artefacts due to the contact between the probe and the edge of the silica bead (the scan direction is from right to left). The modulus distribution are plotted for the two tips (Fig. 9B), when scanning silica is scanned. The means and associated standard deviations, determined for the silica bead locations are  $62 \pm 26$

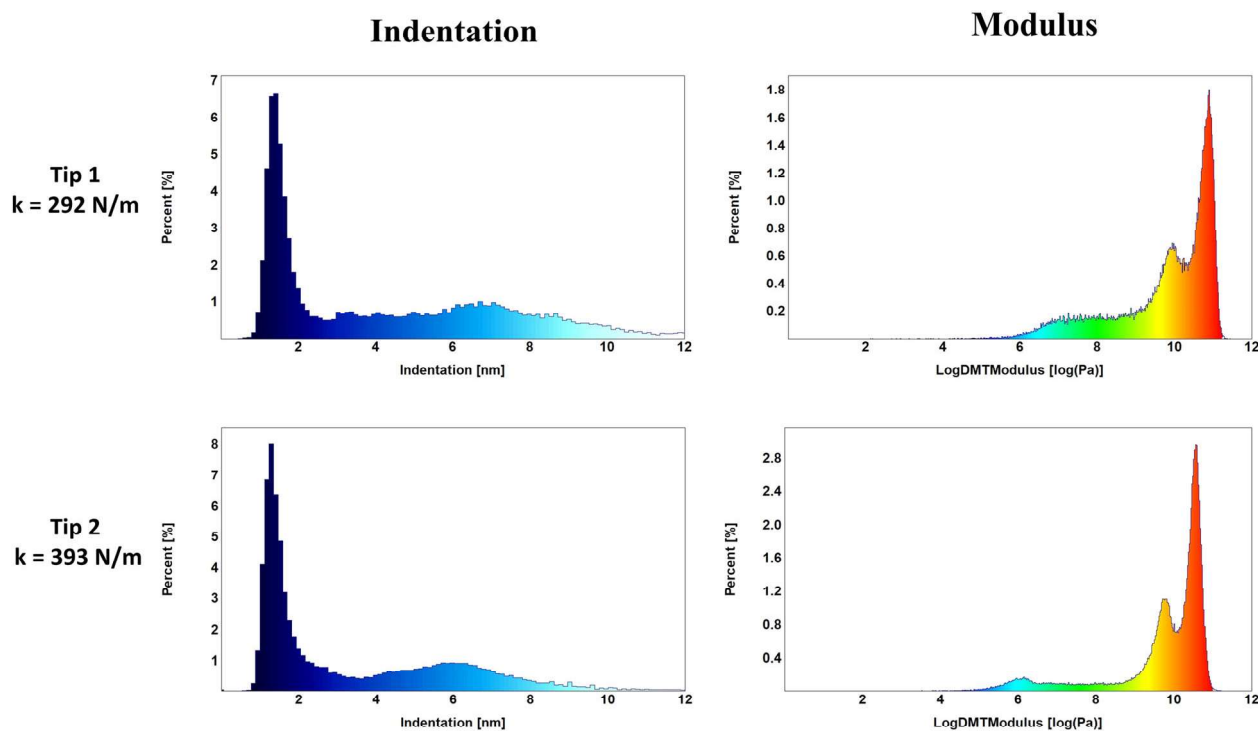


Fig. 9. Analysis of PF-QNM measurements, histograms of (A) indentation and (B) Young's modulus, determined in whole image with the two probes.

and  $84 \pm 22$  GPa for the tip 1 and tip 2, respectively. These differences may be explained by several sources: the thin layer of water at the surface of the sample, the internal compliance, the displacement calibration linearity and also the reliability (Cohen & Kalfon-Cohen, 2013) of the used analytical model. The main result is that the two histograms of modulus show consistent values with the classical nanoindentation testing. Even for relative high modulus values ( $> 50$  GPa), PF-QNM mode provides nanomechanical measurements with a high spatial resolution. The modulus is determined in the elastic region of the load–deformation curve; the methods present the real advantage of being nondestructive and fast.

## Conclusion

In the present work, we have investigated measurements performed on silica beads incorporated in epoxy matrix by means of the advanced AFM technique PF-QNM which, in general, is used to evaluate local mechanical properties of stiff material. Based on the deflection of the AFM cantilever, in interaction with the analysed surface, mappings of local mechanical properties (modulus and indentation) are obtained. The effect of spring constant of two AFM hand-crafted natural full diamond tips with steel cantilevers on the mechanical properties is investigated. The mechanical analysis of incorporated silica beads in an epoxy matrix showed that the signal deformation of the probe, with higher spring constant, leads to a small deformation of the cantilever and then to a lower modulus. It

was concluded that the cantilever spring constant and therefore the proportion of cantilever deflection are indicative of how sensitive any particular probe is when measuring surfaces. It was also observed that topographical surface roughness can influence the mechanical measurements with a variation and population of lower modulus. The AFM nanomechanical mapping (with higher spatial resolution and surface sensitivity), in the elastic region of the sample, has the potential to be a useful supplement to classical instrumented nanoindentation for measuring the Young's modulus. *In fine*, the average values of the contact modulus obtained with the two techniques are virtually comparable, demonstrating that a certain agreement between nanoindentation and PF-QNM exists. This statement is possible because of the nature of the studied materials (which allows the use of the DMT model) and because the viscoelasticity is negligible.

## Acknowledgements

The authors would like to thank CARNOT ESP Institute for supporting the PACK5G research project. Ph.L. is FRS-FNRS senior research associate (Belgium).

## References

- Arnould, O., Siniscalco, D., Bourmaud, A., Le Duigou, A. & Baley, C. (2017) Better insight into the nano-mechanical properties of flax

- fibre cell walls. *Ind. Crops Prod.* **97**, 224–228. <https://doi.org/10.1016/j.indcrop.2016.12.020>.
- Bae, J.W., Kim, W., Hwang, S.C., Choe, Y.S. & Lee, S.-H. (2004) A low-viscosity, highly thermally conductive epoxy molding compound (EMC). *Macromol. Res.* **12**, 78–84. <https://doi.org/10.1007/BF03218998>.
- Bahrami, A., Bailly, C. & Nysten, B. (2019) Spatial resolution and property contrast in local mechanical mapping of polymer blends using AFM dynamic force spectroscopy. *Polymer* **165**, 180–190. <https://doi.org/10.1016/j.polymer.2019.01.023>.
- Baker, S.P. (2001) Nanoindentation techniques. In *Encyclopedia of Materials: Science and Technology* (ed. by K.H.J. Buschow, R.W. Cahn, M.C. Flemings, B. Ilshner, E.J. Kramer, S. Mahajan & P. Veysseyre), pp. 5908–5915. Elsevier, Oxford, ISBN 978-0-08-043152-9.
- Balnois, E., Busnel, E., Baley, C. & Grohens, Y. (2007) An AFM study of the effect of chemical treatments on the surface microstructure and adhesion properties of flax fibres. *Compos. Interf.* **14**, 715–731. <https://doi.org/10.1163/156855407782106537>.
- Bell, M., Krentz, T., Keith Nelson, J. et al. (2017) Investigation of dielectric breakdown in silica-epoxy nanocomposites using designed interfaces. *J. Colloid Interf. Sci.* **495**, 130–139. <https://doi.org/10.1016/j.jcis.2017.02.001>.
- Chandra, R.B.J., Shivamurthy, B., Kulkarni, S.D. & Kumar, M.S. (2019) Hybrid polymer composites for EMI shielding application- a review. *Mater. Res. Express* **6**, 082008. <https://doi.org/10.1088/2053-1591/aaff00>.
- Cohen, S.R. & Kalfon-Cohen, E. (2013) Dynamic nanoindentation by instrumented nanoindentation and force microscopy: a comparative review. *Beilst. J. Nanotechnol.* **4**, 815–833. <https://doi.org/10.3762/bjnano.4.93>.
- Coq Germanicus, R., Leclère, Ph., Guhel, Y., Boudart, B., Touboul, A.D., Descamps, P., Hug, E. & Eyben, P. (2015) On the effects of a pressure induced amorphous silicon layer on consecutive spreading resistance microscopy scans of doped silicon. *J. Appl. Phys.* **117**, 244306. <https://doi.org/10.1063/1.4923052>.
- Coq Germanicus, R., Picard, E., Domenges, B., Danilo, K. & Rogel, R. (2007) Microstructure and electrical characterization based on AFM of very high-doped polysilicon grains. *Appl. Surf. Sci.* **253**, 6006–6012. <https://doi.org/10.1016/j.apsusc.2006.12.114>.
- Cuong, N.T., Barrau, S., Dufay, M. et al. (2020) On the nanoscale mapping of the mechanical and piezoelectric properties of poly (L-Lactic Acid) electrospun nanofibers. *Appl. Sci.* **10**, 652. <https://doi.org/10.3390/app10020652>.
- Derjaguin, B.V., Muller, V.M. & Toporov, Yu.P. (1975) Effect of contact deformations on the adhesion of particles. *J. Colloid Interf. Sci.* **53**, 314–326. [https://doi.org/10.1016/0021-9797\(75\)90018-1](https://doi.org/10.1016/0021-9797(75)90018-1).
- Dittanet, P. & Pearson, R.A. (2012) Effect of silica nanoparticle size on toughening mechanisms of filled epoxy. *Polymer* **53**, 1890–1905. <https://doi.org/10.1016/j.polymer.2012.02.052>.
- Dittanet, P. & Pearson, R.A. (2013) Effect of bimodal particle size distributions on the toughening mechanisms in silica nanoparticle filled epoxy resin. *Polymer* **54**, 1832–1845. <https://doi.org/10.1016/j.polymer.2012.12.059>.
- Doerner, M.F. & Nix, W.D. (1986) A method for interpreting the data from depth-sensing indentation instruments. *J. Mater. Res.* **1**, 601–609. <https://doi.org/10.1557/JMR.1986.0601>.
- Dokukin, M.E. & Sokolov, I. (2012) Quantitative mapping of the elastic modulus of soft materials with HarmoniX and PeakForce QNM AFM Modes. *Langmuir* **28**, 16060–16071. <https://doi.org/10.1021/la302706b>.
- Eyben, P., Vandervorst, W., Alvarez, D., Xu, M. & Fouchier, M. (2007) Probing semiconductor technology and devices with scanning spreading resistance microscopy. In *Scanning Probe Microscopy*, (ed. by S. Kalinin & A. Gruverman), pp. 31–87. Springer, New York, NY.
- Fischer, H., Stadler, H. & Erina, N. (2013) Quantitative temperature-depending mapping of mechanical properties of bitumen at the nanoscale using the AFM operated with PeakForce Tapping™ mode. *J. Microsc.* **250**, 210–217. <https://doi.org/10.1111/jmi.12036>.
- Gan, C.L., Classe, F.C., Chan, B.L. & Hashim, U. (2014) Effects of bonding wires and epoxy molding compound on gold and copper ball bonds intermetallic growth kinetics in electronic packaging. *J. Elec. Mater.* **43**, 1017–1025. <https://doi.org/10.1007/s11664-014-3011-y>.
- Germanicus, R.C., Bourlier, Y., Notot, V. et al. (2020) Three dimensional resistance mapping of self-organized Sr3V2O8 nanorods on metallic perovskite SrVO3 matrix. *Appl. Surf. Sci.* **510**, 145522. <https://doi.org/10.1016/j.apsusc.2020.145522>.
- Granta D. (2019) The material information technology experts. Available at: <https://grantadesign.com/> (accessed on Oct 22, 2019).
- Han, S. & Wang, K.K. (1997) Study on the pressurized underfill encapsulation of flip chips. *IEEE Trans. Comp., Packag., Manufact. Technol.: Part B* **20**, 434–442. <https://doi.org/10.1109/96.641512>.
- Heuberger, M., Dietler, G. & Schlapbach, L. (1995) Mapping the local Young's modulus by analysis of the elastic deformations occurring in atomic force microscopy. *Nanotechnology* **6**, 12–23. <https://doi.org/10.1088/0957-4484/6/1/003>.
- Ho, E. & Marcolongo, M. (2005) Effect of coupling agents on the local mechanical properties of bioactive dental composites by the nano-indentation technique. *Dent. Mater.* **21**, 656–664. <https://doi.org/10.1016/j.dental.2004.09.002>.
- Hopf, J. & Pierce, E.M. (2014) Topography and mechanical property mapping of international simple glass surfaces with atomic force microscopy. *Procedia Mater. Sci.* **7**, 216–222. <https://doi.org/10.1016/j.mspro.2014.10.028>.
- Huang, Z., Wolf, P.D., Poddar, R. et al. (2016) PeakForce scanning electrochemical microscopy with nanoelectrode probes. *Microsc. Today* **24**, 18–25. <https://doi.org/10.1017/S1551929516000882>.
- Khelifa, F., Habibi, Y., Leclère, P. & Dubois, P. (2013) Convection-assisted assembly of cellulose nanowhiskers embedded in an acrylic copolymer. *Nanoscale* **5**, 1082–1090. <https://doi.org/10.1039/C2NR33194B>.
- Kim, H.-S., Huh, J. & Ryu, J. (2010) Investigation of moisture-induced delamination failure in a semiconductor package via multi-scale mechanics. *J. Phys. D: Appl. Phys.* **44**, 034007. <https://doi.org/10.1088/0022-3727/44/3/034007>.
- Kossmann, S., Iost, A., Chicot, D. et al. (2019) Mechanical characterization by multiscale instrumented indentation of highly heterogeneous materials for braking applications. *J. Mater. Sci.* **54**, 4647–4670. <https://doi.org/10.1007/s10853-018-3158-7>.
- Li, C., Ostadhassan, M., Guo, S., Gentzis, T. & Kong, L. (2018) Application of PeakForce tapping mode of atomic force microscope to characterize nanomechanical properties of organic matter of the Bakken Shale. *Fuel* **233**, 894–910. <https://doi.org/10.1016/j.fuel.2018.06.021>.
- Li, H. & Vlassak, J.J. (2009) Determining the elastic modulus and hardness of an ultra-thin film on a substrate using nanoindentation. *J. Mater. Res.* **24**, 1114–1126. <https://doi.org/10.1557/jmr.2009.0144>.

- Li, X. & Bhushan, B. (2002) A review of nanoindentation continuous stiffness measurement technique and its applications. *Mater. Charact.* **48**, 11–36. [https://doi.org/10.1016/S1044-5803\(02\)00192-4](https://doi.org/10.1016/S1044-5803(02)00192-4).
- Li, X., Bhushan, B., Takashima, K., Baek, C.-W. & Kim, Y.-K. (2003) Mechanical characterization of micro/nanoscale structures for MEMS/NEMS applications using nanoindentation techniques. *Ultramicroscopy* **97**, 481–494. [https://doi.org/10.1016/S0304-3991\(03\)00077-9](https://doi.org/10.1016/S0304-3991(03)00077-9).
- Liang, Y.L. & Pearson, R.A. (2009) Toughening mechanisms in epoxy–silica nanocomposites (ESNs). *Polymer* **50**, 4895–4905. <https://doi.org/10.1016/j.polymer.2009.08.014>.
- Lin, Y.C., Weng, Y.J., Pen, D.J. & Li, H.C. (2009) Deformation model of brittle and ductile materials under nano-indentation. *Mater. Design* **30**, 1643–1649. <https://doi.org/10.1016/j.matdes.2008.07.028>.
- Linec, M. & Mušič, B. (2019) The effects of silica-based fillers on the properties of epoxy molding compounds. *Materials (Basel)* **12**, 1811. <https://doi.org/10.3390/ma12111811>.
- Liu, J., Xu, B., Wang, H., Cui, X., Zhu, L. & Jin, G. (2015) Measurement for mechanical behavior and fatigue property of Cu films by nanoscale dynamic load method. *Mater. Design (1980-2015)* **65**, 1136–1142. <https://doi.org/10.1016/j.matdes.2014.08.043>.
- Liu, S.L., Chen, G. & Yong, M.S. (2004) EMC characterization and process study for electronics packaging. *Thin Solid Films* **462–463**, 454–458. <https://doi.org/10.1016/j.tsf.2004.05.080>.
- Lu, X., Xu, L., Lai, H., Du, X., Liu, J. & Cheng, Z. (2009) Studies on microstructure of epoxy molding compound (EMC)–Leadframe interface after environmental aging. In *Proceedings of the 2009 International Conference on Electronic Packaging Technology High Density Packaging*, pp. 1051–1053. Beijing.
- Mercier, D., Vanhumbecq, J.-F., Caruso, M., Eynde, X.V. & Febvre, M. (2019) Microstructural and mechanical characterisation of electroplated nickel matrix composite coatings. *Surf. Eng.* **35**, 177–188. <https://doi.org/10.1080/02670844.2018.1433270>.
- Morales-Rivas, L., González-Orive, A., Garcia-Mateo, C., Hernández-Creus, A., Caballero, E.G. & Vázquez, L. (2015) Nanomechanical characterization of nanostructured bainitic steel: peak force microscopy and nanoindentation with AFM. *Sci. Rep.* **5**, 17164. <https://doi.org/10.1038/srep17164>.
- Murray, H., Germanicus, R., Doukkali, A., Martin, P., Domenges, B. & Descamps, P. (2007) Analytic description of scanning capacitance microscopy. *J. Vacuum Sci. Technol. B: Microelectr. Nanometer Struct. Proc., Measur., Phenom.* **25**, 1340–1352. <https://doi.org/10.1116/1.2759218>.
- Noijen, S., Engelen, R., Martens, J., Opran, A. & van der Sluis, O. (2009) On the epoxy moulding compound aging effect on package reliability. In *Proceedings of the EuroSimE 2009 – 10th International Conference on Thermal, Mechanical and Multi-Physics Simulation and Experiments in Microelectronics and Microsystems*, pp. 1–5. Delft.
- Oh, G.-H., Joo, S.-J., Jeong, J.-W. & Kim, H.-S. (2019) Effect of plasma treatment on adhesion strength and moisture absorption characteristics between epoxy molding compound/silicon chip (EMC/chip) interface. *Microelectron. Reliab.* **92**, 63–72. <https://doi.org/10.1016/j.microrel.2018.11.004>.
- Oliver, W.C. & Pharr, G.M. (1992) An improved technique for determining hardness and elastic modulus using load and displacement sensing indentation experiments. *J. Mater. Res.* **7**, 1564–1583. <https://doi.org/10.1557/JMR.1992.1564>.
- Pharr, G.M. & Oliver, W.C. (1992) Measurement of thin film mechanical properties using nanoindentation. *MRS Bull.* **17**, 28–33. <https://doi.org/10.1557/S0883769400041634>.
- Pittenger, B., Erina, N. & Su, C. (2014) Mechanical property mapping at the nanoscale using peakforce QNM scanning probe technique. In *Nanomechanical Analysis of High Performance Materials* (ed. by A. Tiwari). Solid Mechanics and Its Applications, pp. 31–51. Springer Netherlands, Dordrecht, ISBN 978-94-007-6919-9.
- Preghenella, M., Pegoretti, A. & Migliaresi, C. (2005) Thermo-mechanical characterization of fumed silica-epoxy nanocomposites. *Polymer* **46**, 12065–12072. <https://doi.org/10.1016/j.polymer.2005.10.098>.
- Qi, Y., Jiang, D., Ju, S., Zhang, J. & Cui, X. (2019) Determining the interphase thickness and properties in carbon fiber reinforced fast and conventional curing epoxy matrix composites using peak force atomic force microscopy. *Compos. Sci. Technol.* **184**, 107877. <https://doi.org/10.1016/j.compscitech.2019.107877>.
- Rector, L.P., Gong, S., Miles, T.R. & Gaffney, K. (2000) Transfer molding encapsulation of Flip Chip array packages. In *Proceedings-SPIE the International Society for Optical Engineering*, pp. 760–767. International Society for Optical Engineering, 1999.
- Smolyakov, G., Formosa-Dague, C., Séverac, C., Duval, R.E. & Dague, E. (2016) High speed indentation measures by FV, QI and QNM introduce a new understanding of bionanomechanical experiments. *Micron* **85**, 8–14. <https://doi.org/10.1016/j.micron.2016.03.002>.
- Smolyakov, G., Pruvost, S., Cardoso, L., Alonso, B., Belamie, E. & Duchet-Rumeau, J. (2016) AFM PeakForce QNM mode: evidencing nanometre-scale mechanical properties of chitin-silica hybrid nanocomposites. *Carbohydr. Polym.* **151**, 373–380. <https://doi.org/10.1016/j.carbpol.2016.05.042>.
- Sriwithoon, N., Ugsornrat, K., Srisuwitthanon, W. & Thonglor, P. (2017) Warpage of QFN package in post mold cure process of integrated circuit packaging. *J. Phys.: Conf. Ser.* **901**, 012089. <https://doi.org/10.1088/1742-6596/901/1/012089>.
- Tachapitunsuk, J., Ugsornrat, K., Srisuwitthanon, W. & Thonglor, P. (2017) Effecting aging time of epoxy molding compound to molding process for integrated circuit packaging. *J. Phys.: Conf. Ser.* **901**, 012090. <https://doi.org/10.1088/1742-6596/901/1/012090>.
- Trtik, P., Kaufmann, J. & Volz, U. (2012) On the use of peak-force tapping atomic force microscopy for quantification of the local elastic modulus in hardened cement paste. *Cem. Concr. Res.* **42**, 215–221. <https://doi.org/10.1016/j.cemconres.2011.08.009>.
- Tsai, M.-, Wang, C.T. & Hsu, C.H. (2006) The effect of epoxy molding compound on thermal/residual deformations and stresses in IC packages during manufacturing process. *IEEE Trans. Compon. Packag. Technol.* **29**, 625–635. <https://doi.org/10.1109/TCAPT.2006.880478>.
- Ureña, A., Rams, J., Escalera, M.D. & Sánchez, M. (2005) Characterization of interfacial mechanical properties in carbon fiber/aluminium matrix composites by the nanoindentation technique. *Compos. Sci. Technol.* **65**, 2025–2038. <https://doi.org/10.1016/j.compscitech.2005.04.013>.
- Vandervorst, W., Fleischmann, C., Bogdanowicz, J., Franquet, A., Celano, U., Paredis, K. & Budrevich, A. (2017) Dopant, composition and carrier profiling for 3D structures. *Mater. Sci. Semicond. Process.* **62**, 31–48. <https://doi.org/10.1016/j.mssp.2016.10.029>.
- Walczyk, W., Schön, P.M., Schönherr, H. (2013) The effect of Peak-Force tapping mode AFM imaging on the apparent shape of surface

- nanobubbles. *J. Phys.: Condens. Matter* **25**, 184005. <https://doi.org/10.1088/0953-8984/25/18/184005>.
- Wang, H., Bai, Y., Liu, S., Wu, J. & Wong, C.P. (2002) Combined effects of silica filler and its interface in epoxy resin. *Acta Mater.* **50**, 4369–4377. [https://doi.org/10.1016/S1359-6454\(02\)00275-6](https://doi.org/10.1016/S1359-6454(02)00275-6).
- Wong, K.J., Low, K.O., Israr, H.A. & Tamin, M.N. (2016) Thickness-dependent non-Fickian moisture absorption in epoxy molding compounds. *Microelectron. Reliab.* **65**, 160–166. <https://doi.org/10.1016/j.microrel.2016.08.014>.
- Xu, L., Guo, Q., Qian, S. & Wu, S. (2018) Self-adaptive grinding for blind tip reconstruction of AFM diamond probe. *Nanotechn. Prec. Eng.* **1**, 150–155. <https://doi.org/10.13494/j.npe.20170010>.
- Young, T.J., Monclus, M.A., Burnett, T.L., Broughton, W.R., Ogin, S.L. & Smith, P.A. (2011) The use of the PeakForce™ quantitative nanomechanical mapping AFM-based method for high-resolution Young's modulus measurement of polymers. *Meas. Sci. Technol.* **22**, 125703. <https://doi.org/10.1088/0957-0233/22/12/125703>.
- Zeng, G., Dirscherl, K. & Garnæs, J. (2018) Toward accurate quantitative elasticity mapping of rigid nanomaterials by atomic force microscopy: effect of acquisition frequency, loading force, and tip geometry. *Nanomaterials (Basel)* **8**, 616 <https://doi.org/10.3390/nano8080616>.
- Zhang, Z. & Wong, C.P. (2004) Recent advances in flip-chip underfill: materials, process, and reliability. *IEEE Trans. Adv. Packag.* **27**, 515–524. <https://doi.org/10.1109/TADVP.2004.831870>.